Electronic and Structural Evolution of Monoiron Sulfur Clusters, FeS_n^- and FeS_n (n = 1−6), from Anion Photoelectron Spectroscopy

Hua-Jin Zhai, Boggavarapu Kiran, and Lai-Sheng Wang*

Department of Physics, Washington State University, 2710 University Drive, Richland, Washington 99352, and W. R. Wiley Environmental Molecular Sciences Laboratory, Pacific Northwest National Laboratory, MS K8-88, P.O. Box 999, Richland, Washington 99352

Received: December 31, 2002; In Final Form: February 19, 2003

We report a photoelectron spectroscopic investigation of a series of monoiron−sulfur clusters FeS_n^- (n = 1−6) at various photon energies. Vibrationally resolved spectra were measured for FeS^- and FeS_3^-. A wealth of electronic structure information was obtained for FeS and were tentatively assigned, yielding a $^5\Delta$ ground state for FeS and a $^7\Sigma^+$ and a $^5\Delta$ excited state at 0.675 and 1.106 eV above the ground state, respectively. Franck−Condon factor simulations were performed for the vibrationally resolved $^5\Delta$ ground state and the $^5\Delta$ excited state, yielding an Fe−S bond length of 2.18 and 2.29 Å for the anion ground state and the $^5\Delta$ excited state, respectively, as well as a vibrational temperature of 180 K for the anion. The electron affinities (EA's) of FeS_n were measured to be 1.725 ± 0.10, 3.222 ± 0.009, 2.898 ± 0.008, 3.129 ± 0.008, 3.262 ± 0.010, and 3.52 ± 0.02 eV for n = 1−6, respectively. A significant EA increase was only observed from FeS to FeS_2, whereas all larger species FeS_n (n = 3−6) possess EA's similar to that of FeS_2 within ±0.3 eV. By comparing the trend of EA in FeS_n to that of FeO_n, we proposed that all the FeS_n^- (n > 1) species take $(S_m^{2-})Fe^{3+}(S_{n-m}^{2-})$ type structures, in which Fe assumes its favorite +3 formal oxidation state. Preliminary density functional calculations were carried out and the obtained structures support the proposed structural evolution of the FeS_n^- clusters.

1. Introduction

Iron−sulfur clusters are prevalent throughout bioinorganic chemistry.[1] Abiological investigations of iron−sulfur clusters and complexes[2−5] provide fundamental information about the structural, electronic, and magnetic properties, and chemical bonding of the Fe−S systems. A large number of iron−sulfur clusters and complexes have been synthesized and characterized, forming a large class of organometallic chemistry.[2] There have also been extensive theoretical efforts devoted to iron−sulfur complexes.[3−5] However, there have been relatively few studies on the bare Fe−S clusters; even the electronic structure of the simplest FeS diatomic molecule is still not well understood. We are interested in probing the electronic structure and chemical bonding of a broad range of iron−sulfur systems in the gas phase using photoelectron spectroscopy (PES), ranging from bare Fe−S clusters produced using a laser vaporization source[6] to analogue complexes and proteins using an electrospray ionization source.[7] In the current paper, we focus on a series of relatively simple bare iron−sulfur clusters, the monoiron sulfur clusters FeS_n^- (n = 1−6).

There have been numerous experimental and theoretical reports on the monoiron−sulfur clusters in the literature. DeVore et al. reported a vibrational frequency of 540 cm^{-1} for neutral diatomic FeS using matrix infrared spectroscopy.[8] The reactions of FeS^+ with D_2 and methane were examined by Barsch et al. using guided-ion beam mass spectrometry.[9,10] Photodissociation spectra of FeS^+ were measured by Hettich et al.[11] and Husband et al.[12] Schröder et al. have reported a detailed study on the structures of cationic, anionic, and neutral FeS_2 using both mass spectrometric methods and density functional theory (DFT) calculations.[13] Sequential reactions of Fe^+ with ethylene sulfide were conducted to generate FeS_n^+ species, and at least six sulfur attachments were observed.[14] Bare Fe^+ ions were also allowed to react with S_8 in the gas phase using a Fourier transform ion cyclotron resonance mass spectrometer to produce FeS_n^+ clusters,[15,16] and species with n up to 10 were observed. Photodissociation and collision-induced dissociation (CID) experiments were carried out on FeS_n^+ (n = 1−6) by MacMahon et al.,[17] and on FeS_n^+ (n = 2−8) by Yu et al.[18] Anionic FeS_6^- and FeS_7^- were also investigated by CID, and loss of neutral S_2 fragments were observed as a major dissociation channel.[19] Low resolution photoelectron spectra of FeS_n^- (n = 1−6) at 266 nm were reported by Kaya and co-workers.[20] Theoretical treatment of iron−sulfur clusters has been challenging.[3−5,21−26] Even the electronic structure and chemical bonding in the diatomic FeS were not well understood at present despite much effort in the past decade.[21−25] Except for the DFT calculations of FeS_2 by Schröder et al.,[13] there is no other theoretical studies on any other lager FeS_n clusters.

In this paper, we report a detailed photoelectron spectroscopic study of a series of monoiron−sulfur clusters: FeS_n^- (n = 1−6). Vibrationally resolved PES spectra and studies at various photon energies allow a wealth of information on the structural and electronic evolution and chemical bonding in the monoiron−sulfur clusters to be obtained. The FeS_n^- clusters were compared with the FeO_n^- species and they were proposed to have $(S_m^{2-})Fe^{3+}(S_{n-m}^{2-})$ types of structures, in which the Fe atom assumes its favorite formal oxidation state of +3. A preliminary DFT study was carried out on the structures of FeS_n^- and the DFT results are consistent with the proposed structural evolution for the monoiron−sulfur clusters.

* Corresponding author. E-mail: ls.wang@pnl.gov.

10.1021/jp027867z CCC: $25.00
Published on Web 03/27/2003

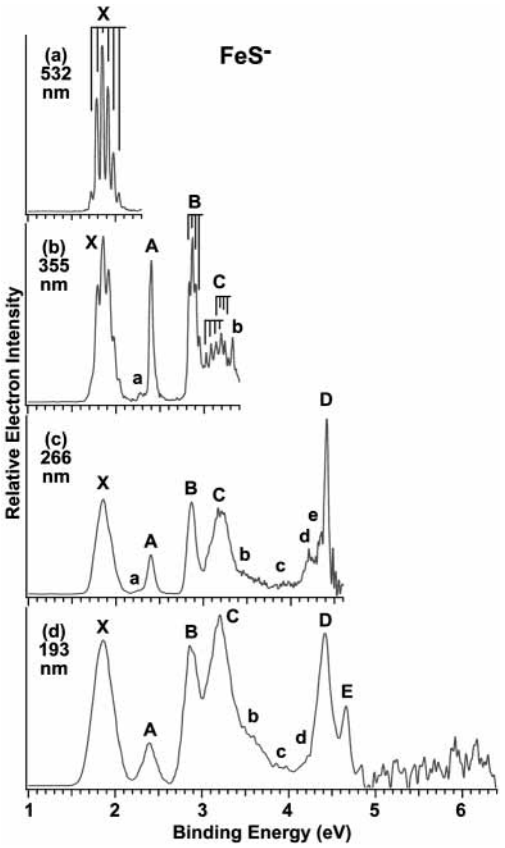

Figure 1. Photoelectron spectra of FeS^- at (a) 532 nm (2.331 eV), (b) 355 nm (3.496 eV), (c) 266 nm (4.661 eV), and (d) 193 nm (6.424 eV). The vertical lines represent vibrational structures.

2. Experimental Method

The experiment was carried out using a magnetic-bottle time-of-flight PES apparatus equipped with a laser vaporization supersonic cluster source.[6] Briefly, a mixed Fe/S target (10/1 molar ratio) was laser-vaporized in the presence of a helium carrier gas. Various $Fe_mS_n^-$ clusters were produced from the cluster source and were mass analyzed using a time-of-flight mass spectrometer. The FeS_n^- ($n = 1-6$) species of our current interest were mass-selected and decelerated before being photodetached. Four detachment photon energies were used in the current experiments: 532 nm (2.331 eV), 355 nm (3.496 eV), and 266 nm (4.661 eV) from a Nd:YAG laser, and 193 nm (6.424 eV) from an ArF excimer laser. Photoelectrons were collected at nearly 100% efficiency by the magnetic bottle and analyzed in a 3.5 m long electron flight tube. The photoelectron spectra were calibrated using the known spectrum of Rh^-, and the resolution of the apparatus was $\Delta Ek/Ek \sim 2.5\%$, i.e., ~25 meV for 1 eV electrons. The electron binding energies (BE) were determined from the photoelectric equation: $BE = h\nu - Ek$.

3. Results

The obtained PES spectra for FeS_n^- ($n = 1-6$) at different photon energies are shown in Figures 1−6, respectively. The observed detachment transitions are labeled with letters and the vertical lines represent the resolved vibrational structures. Figure 7 compares the spectra of all six species at 193 nm.

3.1. FeS^-. The PES spectra of FeS^- were measured at four photon energies, as shown in Figure 1. At the highest photon energy used (Figure 1d), six intense and well-resolved features (X, A−E) were observed, with several weak features (a−d). The 532 nm spectrum (Figure 1a) revealed a long and well-resolved vibrational progression for the ground-state transition (X) with an average spacing of 520 ± 30 cm^{-1}. The 0−0 transition was weak, defining an adiabatic detachment energy (ADE) of 1.725 ± 0.010 eV, which represents the electron affinity (EA) of the neutral FeS molecule. The vertical detachment energy (VDE) was defined by the 2 ←0 transition at 1.851 ± 0.010 eV.

The 355 nm spectra (Figure 1b) revealed several more transitions. The feature A with a VDE of 2.400 ± 0.008 eV was very sharp, only slightly broader than the instrumental resolution. The next low-lying transition (B) showed a simple and well-resolved vibrational progression with an average spacing of 325 ± 30 cm^{-1}. The ADE for the B band was measured to be 2.831 ± 0.009 eV. At the higher binding energy side of the 355 nm spectrum, numerous peaks were observed. The six peaks in band C appeared to consist of a vibrational progression, but their spacings are not equal. The first three peaks gave an average spacing of 450 ± 40 cm^{-1}, whereas the three higher binding energy peaks yielded an average spacing of 330 ± 40 cm^{-1}. The relative intensity of the C band increased at higher photon energies (Figure 1c,d), where a single unresolved band was observed due to the deterioration of spectral resolution at higher electron kinetic energies. A sharp peak at 3.32 eV (labeled b) was also observed in the 355 nm spectrum (Figure 1b), but its intensity seemed to be significantly reduced in the higher photon energy spectra.

At 266 nm, an intense and sharp peak (D) was observed at the high binding energy end with a VDE of 4.413 ± 0.010 eV. In addition, numerous weak and diffuse features were observed between 3.4 and 4.4 eV. At 193 nm, one more sharp peak (E) was observed at a VDE of 4.66 eV. At higher binding energies beyond 4.7 eV, no intense transitions were revealed. There might be weak spectral features, but the signal-to-noise ratio was too poor to allow any definitive identification in the high binding energy range. The binding energies and vibrational frequencies for the major spectral features observed for FeS^- are summarized in Table 1, along with tentative assignments, which will be discussed later.

3.2. FeS_2^-. The PES spectra of FeS_2^- measured at three photon energies are shown in Figure 2. Six intense and well-resolved bands (X, A−E) were observed at 193 nm (Figure 2c). The relative intensities of the bands A, B, and C decreased at 266 nm (Figure 2b). These bands were rather congested and were not better resolved under the improved instrumental resolution afforded at 266 nm. However, the X band was resolved into several features under the improved resolution at 355 nm (Figure 2a). These peaks appeared to consist of a vibrational progression, but their spacings were not uniform, indicating that probably more than one vibrational mode was involved. The threshold peak in the 355 nm spectrum defined a relatively accurate EA for FeS_2 at 3.222 ± 0.009 eV, which is much higher than that of FeS. Close examination of the 355 nm spectrum revealed that very weak features (X′ and A′) were present in the lower binding energy side. These features, which accounted for about 1% of the intensity relative to that of the X band, depended on the source conditions slightly, but could not be completely eliminated. They were attributed to the existence of a minor isomer, with an ADE of 2.05 ± 0.09 eV and a VDE of 2.15 ± 0.05 eV, much lower than those of the main isomer. The binding energies of all the observed detachment transitions for FeS_2^- are give in Table 2.

3.3. FeS_3^-. The spectra of FeS_3^- are shown in Figure 3 at three photon energies. The 355 nm spectrum (Figure 3a)

TABLE 1: Observed Adiabatic (ADE) and Vertical (VDE) Electron Binding Energies from the Photoelectron Spectra of FeS^- and the Electronic Excitation Energies and Vibrational Frequencies Determined for FeS and Tentative Spectral Assignments[a]

	state	electron configuration	ADE (eV)	VDE (eV)	term value (eV)	vib freq (cm^{-1})
X	$^5\Delta$	$10\sigma^2 4\pi^4 11\sigma^1 5\pi^2 1\delta^3 12\sigma^0$	1.725 (10)	1.851 (10)	0	520 (30)[b]
A	$^7\Sigma^+$	$10\sigma^2 4\pi^4 11\sigma^1 5\pi^2 1\delta^2 12\sigma^1$	2.400 (8)	2.400 (8)	0.675	
B	$^5\Delta$	$10\sigma^2 4\pi^4 11\sigma^0 5\pi^2 1\delta^3 12\sigma^1$	2.831 (9)	2.867 (9)	1.106	325 (30)
C	$^5\Pi$	$10\sigma^2 4\pi^4 11\sigma^1 5\pi^1 1\delta^3 12\sigma^1$	3.025 (10)	3.079 (10)	1.300	450 (40)
	$^5\Phi$		3.150 (15)	3.195 (15)	1.425	330 (40)
D	$^7\Phi$	$10\sigma^2 4\pi^3 11\sigma^1 5\pi^2 1\delta^3 12\sigma^1$	4.413 (10)	4.413 (10)	2.688	
E	$^7\Delta$	$10\sigma^1 4\pi^4 11\sigma^1 5\pi^2 1\delta^3 12\sigma^1$	4.660 (20)	4.660 (20)	2.935	

[a] Numbers in the parentheses indicate the uncertainties of the last digits. [b] 540 cm^{-1} from ref 8.

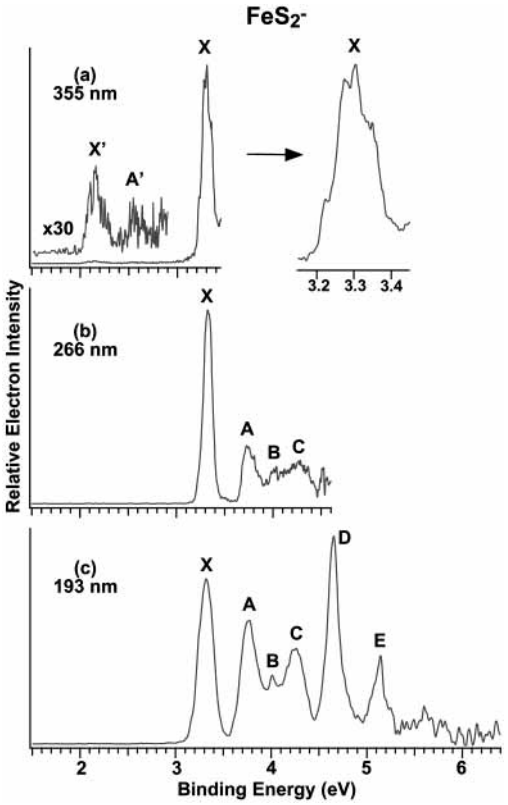

Figure 2. Photoelectron spectra of FeS_2^- at (a) 355 nm, (b) 266 nm, and (c) 193 nm. The inset in (a) shows the fine structures of band X.

displayed surprisingly a simple and well-resolved vibrational progression for the ground-state transition (*X*) with a spacing of 500 ± 20 cm^{-1}. The 0−0 transition defined an accurate EA of 2.898 ± 0.008 eV for neutral FeS_3. At 266 nm, three strong bands (A, B, C) were observed with several weak features (a, b, c). The C band was relatively sharp, but fine features were discernible in the A and B bands, which can be due to either vibrational structures or overlapping electronic transitions. At 193 nm, a broad band (D) was observed between 4.9 and 5.5 eV, which likely contained several overlapping detachment transitions. The binding energies for the major detachment transition of FeS_3^- are listed in Table 2.

3.4. FeS_4^-. Figure 4 shows the PES spectra of FeS_4^- at three photon energies. At 193 nm (Figure 4c), at least seven detachment bands could be identified (X, A−F). The A band appeared as a shoulder on the high binding energy side of band X, whereas the C, D, and E bands overlapped with each other. The F band at higher binding energies was relatively weak and contained at least four discernible features between 5.0 and 5.6 eV. The spacings between the fine features in the F band were too large to be due to a single vibrational progression. The X band was resolved into many fine features under the improved resolution at 355 nm (Figure 4a). At least seven fine features

TABLE 2: Observed Electron Binding Energies (VDEs) for FeS_n^- (n = 2−6), and Adiabatic Electron Affinities (EAs) and Vibrational Frequencies for FeS_n (n = 2−6)[a]

species	obsd feature		EA (eV)	VDE (eV)	vib freq (cm^{-1})
FeS_2^-	X		3.222 (9)	3.306 (9)	
	A			3.75 (3)	
	B			4.01 (2)	
	C			4.25 (2)	
	D			4.66 (2)	
	E			5.15 (2)	
	X′		2.05 (9)	2.15 (5)	
FeS_3^-	X		2.898 (8)	2.898 (8)	500 (20)
	A			3.348 (10)	
	B			4.156 (10)	
	C			4.40 (2)	
	D			4.9−5.5	
FeS_4^-	X	a	3.129 (8)	3.129 (8)	
		b		3.156 (9)	
		c		3.201 (8)	
		d		3.225 (8)	
		e		3.273 (8)	
		f		3.294 (8)	
		g		3.372 (8)	
	A			∼3.5	
	B			3.94 (3)	
	C			∼4.6	
	D			4.76 (3)	
	E			4.89 (3)	
	F			5.0−5.6	
FeS_5^-	X		3.262 (10)	3.262 (10)	510 (40)
	A			3.55 (4)	
	B			4.72 (4)	
	C			5.32 (2)	
	D			∼5.85	
FeS_6^-	X		3.52 (2)	3.52 (2)	
	A			∼3.7	
	B			4.10 (3)	
	C			4.40 (3)	
	D			4.62 (3)	

[a] The numbers in the parentheses represent the experimental uncertainty in the last digitals.

were identified (a−g). The threshold peak a was very sharp and defined an accurate EA of 3.129 ± 0.008 eV for neutral FeS_4. The fine features in the X band could be due to overlapping vibronic states. There appeared to be two vibrational progressions: one consisted of peak a, c, and e (average spacing, 580 ± 40 cm^{-1}) whereas the other one consisted of peak b, d, and f (average spacing, 560 ± 40 cm^{-1}). However, the peak f at 3.294 eV was significantly enhanced in the 266 nm spectrum (Figure 4b), suggesting that it may be a separate detachment channel. On the lower binding energy side in the 355 nm spectrum (Figure 4a), very weak signals were present, which were probably due to contributions from a minor isomer. The binding energies of all the observed features in the spectra of FeS_4^- are also given in Table 2.

3.5. FeS_5^- and FeS_6^-. The PES spectra of FeS_5^- were measured at three photon energies, as shown in Figure 5. The 193 nm spectrum (Figure 5c) exhibited five broad and intense

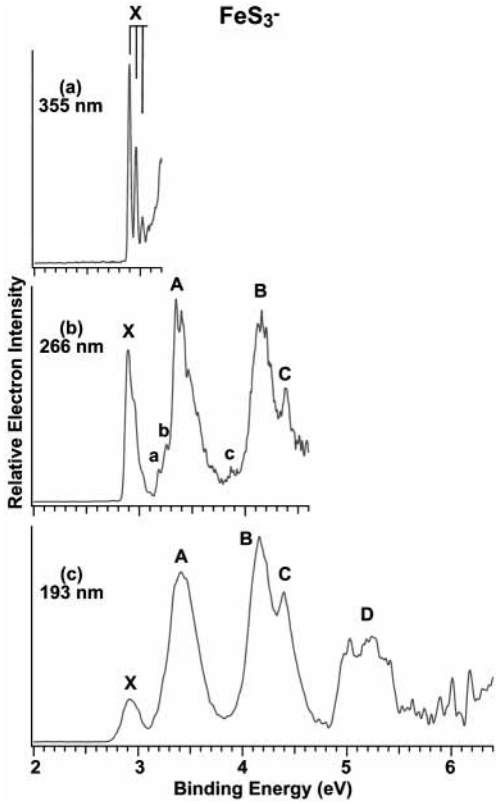

Figure 3. Photoelectron spectra of FeS_3^- at (a) 355 nm, (b) 266 nm, and (c) 193 nm. The vertical lines represent vibrational structures.

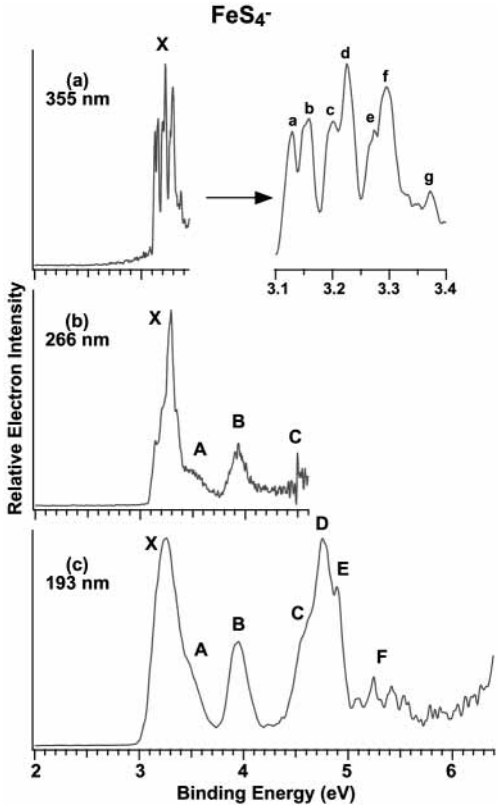

Figure 4. Photoelectron spectra of FeS_4^- at (a) 355 nm, (b) 266 nm, and (c) 193 nm. The inset in (a) shows the fine structures of band *X*.

bands (X, A−D). In the 355 nm spectrum (Figure 5a), a simple vibrational progression was resolved for the ground-state transition (X), with a spacing of 510 ± 40 cm^{-1} and an ADE of 3.262 ± 0.010 eV. The A band, which overlapped with the

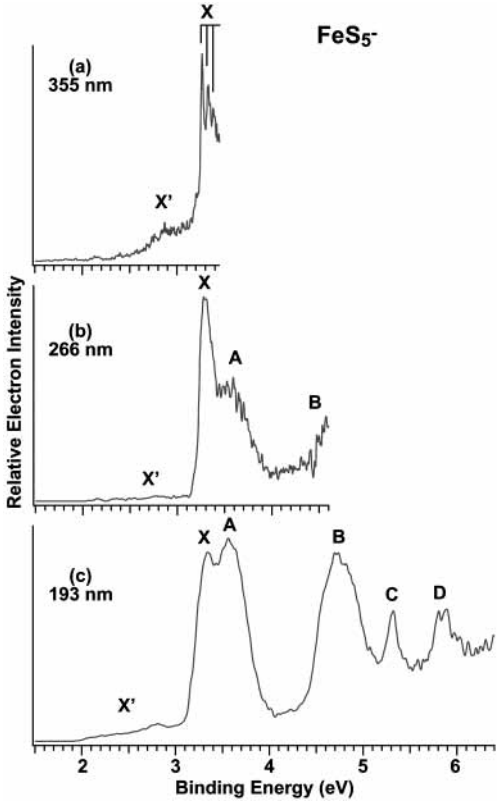

Figure 5. Photoelectron spectra of FeS_5^- at (a) 355 nm, (b) 266 nm, and (c) 193 nm.

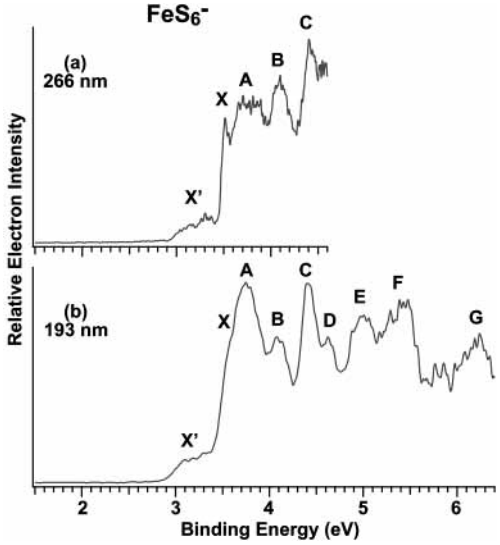

Figure 6. Photoelectron spectra of FeS_6^- at (a) 266 nm and (b) 193 nm.

X band, was enhanced in the 193 nm spectrum. The B, C, D bands have relatively high binding energies and were well separated from the A band. Weak features (X′) at the lower binding energy side, due to the presence of a minor isomer, were observed in the spectra at all three photon energies. Again, the binding energies of the main detachment features of FeS_5^- are given in Table 2.

Due to its high electron binding energies, the spectra of FeS_6^- were taken only at 266 and 193 nm, as shown in Figure 6. Very congested and complex spectra were observed for FeS_6^-. The weak low binding energy features (X′) between 3.0 and 3.4 eV were again attributed to contributions from a minor isomer. Thus, the X feature defines the ground-state transition of the

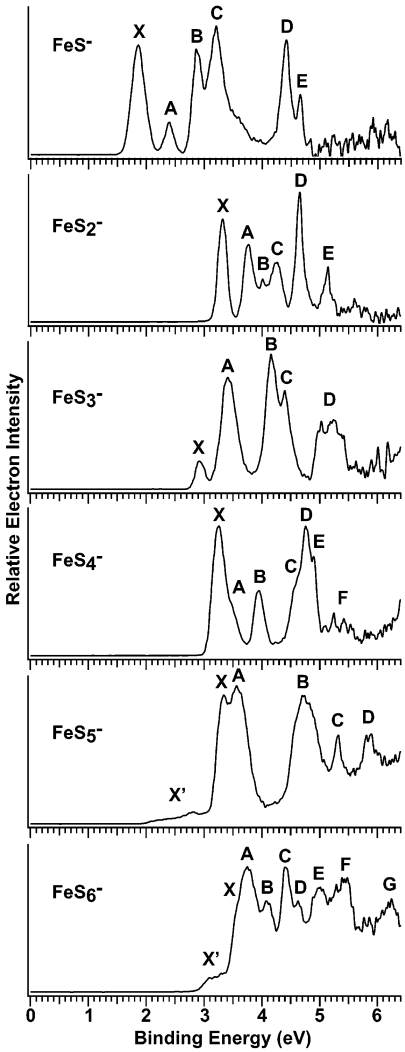

Figure 7. Comparison of the 193 nm photoelectron spectra of FeS_n^- ($n = 1-6$).

main FeS_6^- isomer. This feature was well resolved in the 266 nm spectrum, yielding an ADE of 3.52 ± 0.02 eV. All the higher energy features were broad, and Table 2 lists tentatively the binding energies for some of those bands.

4. Discussion

The PES spectra shown in Figures 1−6 represent detachment transitions from the FeS_n^- anions to the various states of the FeS_n neutrals. They reveal information about the electronic structure and chemical bonding of the monoiron sulfur clusters. However, except for FeS and FeS_2 there have been few theoretical studies on the structure and bonding of these species. In particular, the electronic structures of these species are extremely complex and very little is known for this series of species besides FeS. We will discuss the spectra of FeS^- in more detail and attempt to make some tentative assignments. For the larger clusters, we will discuss only qualitatively the trend of the spectra and the possible structural implications. No detailed spectral assignments are possible at present. We will also present a preliminary density functional theory (DFT) calculations for the species with $n > 1$ to obtain structural information and provide insight into the bonding of the larger FeS_n clusters.

4.1. Electronic Structure and Chemical Bonding in Diatomic FeS^- and FeS. There have been a number of theoretical calculations on the electronic structure of FeS and FeS^-.[21−25]

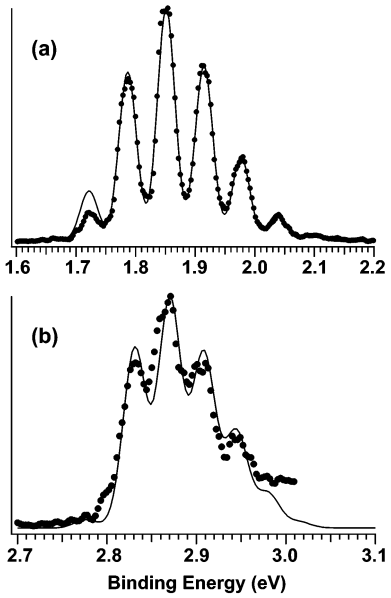

Figure 8. Franck−Condon factor simulations for (a) the X band and (b) the B bands of FeS^- (see Figure 1). The following parameters were used for the simulations: (a) anion frequency 450 cm^{-1}, anharmonicity 5 cm^{-1}, bond length 2.18 Å; neutral frequency, 540 cm^{-1}, anharmonicity, 5 cm^{-1}, bond length, 2.04 Å; anion vibrational temperature 180 K; line width 35 meV; (b) anion frequency 450 cm^{-1}, anharmonicity 5 cm^{-1}, bond length 2.18 Å; neutral frequency 325 cm^{-1}, anharmonicity 5 cm^{-1}, bond length 2.29 Å; anion vibrational temperature 180 K; line width 30 meV.

The ground state of FeS is known to be $^5\Delta$ with an electron configuration of $10\sigma^2 4\pi^4 11\sigma^1 5\pi^2 1\delta^3$, where the 10σ and 4π are weakly bonding MOs mainly of S 3p character, the 11σ is a bonding MO mainly of Fe 3d character, the 5π is an antibonding MO of Fe 3d character, and the 1δ is an Fe 3d nonbonding MO. The recent calculations by Hubner et al. give a $^5\Sigma^+$ ground state for FeS,[25] but the $^5\Delta$ state is predicted to be very closely spaced and the energy difference between the two states is well within the accuracy of the calculations. In the FeS^- anion, the extra electron enters the 12σ orbital, which is an antibonding MO mainly of Fe 4*s* character, to give a $^6\Delta$ state with an electron configuration of $10\sigma^2 4\pi^4 11\sigma^1 5\pi^2 1\delta^3 12\sigma^1$. Because there is little experimental information about the excited states of FeS, we will use the available theoretical information as guidance to give tentative assignments of the major observed PES features.

4.1.1. Ground-State Transition (X) and Franck−Condon Factor Simulations. Feature X represents detachment of the extra electron from the 12σ MO of the anion, leading to the neutral ground state ($^5\Delta$). The broad vibrational progression is consistent with the antibonding nature of the 12σ orbital. Our observed average vibrational spacing of 520 ± 30 cm^{-1} is in excellent agreement with the known vibrational frequency of FeS (540 cm^{-1}).[8] The well-resolved vibrational progression for the ground state afforded us an opportunity to perform a Franck−Condon factor simulation,[27] which would confirm the spectroscopic constants of the ground states of FeS^- and FeS and allow us to estimate the vibrational temperature of FeS^-. We should point out that the $^5\Delta$ state should have a significant spin−orbit splitting yielding a doublet for each vibrational peak in the PES spectra of the X band. However, the spin−orbit components were not resolved due to the limited resolution. The line width of the 532 nm spectrum (Figure 1a) was about 35 meV (fwhm), which was broader than our instrumental resolution, most likely as a result of the spin−orbit broadening.

Figure 8a displays the simulated spectrum, using a Morse oscillator,[27] compared to the experimental data. We used the

known vibrational frequency (540 cm^{-1})[8] and bond length (2.04 Å)[25] of the neutral ground state and a 5 cm^{-1} anharmonicity for both the anion and the neutral. The simulation yielded a bond length of 2.18 Å and a vibrational frequency of 450 cm^{-1} for the FeS^- anion, which are in good agreement with those calculated recently.[25] The anion vibrational frequency for FeS^- is only an estimate because there is very little hot band transition. Most interestingly, we obtained a vibrational temperature of 180 K for FeS^-, the coldest vibrational temperature that we have been able to achieve from our laser vaporization source.[28,29]

4.1.2. The A, B, and C Bands. The A band is very sharp without any vibrational structures and is clearly from removal of a nonbonding electron. It should be due to detachment of a 1δ electron unambiguously, yielding the $^7\Sigma^+$ excited state of FeS at an excitation energy of 0.675 eV relative to the ground state (Table 1). The sharp detachment peak of the A band suggests that the bond length and vibrational frequency of the $^7\Sigma^+$ excited state should be very similar or nearly identical to those of the anion ground state.

The band B exhibited a single vibrational progression with a frequency of 325 cm^{-1}, which is much smaller than that of the ground state of either the neutral or the anion, indicating the detachment of a strongly bonding electron. We assign this band to the detachment of the 11σ orbital, an Fe−S bonding MO, yielding the $^5\Delta$ excited state of FeS with an excitation energy of 1.106 eV (Table 1). Using the spectroscopic constants and the vibrational temperature of the anion ground state, we performed a Franck−Condon factor simulation similar to that for the *X* band, as shown in Figure 8b. We obtained a bond length of 2.29 Å for the $^5\Delta$ excited state of FeS from the Franck−Condon factor simulation. Figure 8b shows that there appeared to be a lower binding energy component in each vibrational peak, possibly due to the spin−orbit splitting expected for the $^5\Delta$ excited state.

The C band is more complicated and not straightforward to assign. In the 266 nm spectrum, numerous vibronic peaks were resolved in this band, which appeared to contain two vibrational progressions. This band is tentatively assigned to be due to detachment from the 5π orbital, yielding the $^5\Pi$ and $^5\Phi$ excited states of FeS, both of which can be produced from a single electron detachment from the 5π orbital.

4.1.3. D and E Bands. The next strong detachment feature is the D band at an ADE of 4.413 eV. We assign this feature to be from detachment of a $4\pi\ \beta$ electron, giving rise to the $^7\Phi$ excited state of FeS at an excitation energy of 2.688 eV (Table 1). This band is quite sharp without significant vibrational structures, suggesting that the 4π orbital is relatively nonbonding. The band E with the highest binding energy could be either due to the $^5\Phi$ state from detachment of a $4\pi\ \alpha$ electron or due to detachment of a $10\sigma\ \beta$ electron, yielding a $^7\Delta$ excited state of FeS. We tentatively assigned the E band to the latter, as shown in Table 1.

4.1.4. Weak PES Features. The above assignments accounted for all the major PES features observed for FeS^-. It is expected that there would be many low-lying excited states for FeS with different spins or angular momenta. However, only those states that involve detachment of a single electron from the anion ground state would give strong PES features. States involving excitations of more than one electron would have much weaker intensities. The relatively weak features (a−d) observed in the spectra of FeS^- are attributed to such multielectron transitions.

Our overall spectral assignments are given in Table 1. All but the X, A, and B bands should be regarded as tentative. We note that our assignments differ significantly from those by Hubner et al.[25] However, those assignments were based on a poorly resolved spectrum[20] and were problematic in themselves. For example, three distinct electronic states ($^5\Sigma^+$, $^5\Delta$, $^7\Sigma^+$) were assigned to the X band on the basis of shoulders observed in the previous spectrum. Our data showed clearly that the X band contains only one vibrational progression. On the basis of the nature of the MOs and the geometry and vibrational frequency changes, we consider the assignments of the X, A, and B states reasonably firm. Our spectra and the Franck−Condon factor simulations yielded a set of spectroscopic constants for these three states, which should provide good experimental references to verify further and more accurate theoretical calculations.

4.2. FeS_2^- and FeS_2. Two structures are possible for FeS_2, a bent structure without S−S bonding or a triangular structure with a S−S bond. The recent work by Schröder et al. reported an extensive experimental and theoretical investigation on the structures of $FeS_2^{+/0/-}$.[13] Their DFT calculation showed that FeS_2^- has a bent structure ($^6A_1$) with a ∠SFeS angle of 166.7° and an Fe−S bond length of 2.12 Å. Their predicted neutral FeS_2 also has a bent structure ($^5B_2$), but it has a large bond angle change (∠SFeS = 115.2°), as well as a bond length change (r_{Fe-S} = 2.03 Å).

The X band in the PES spectrum of FeS_2^- (Figure 2) represents the transition from the ground state of the anion to that of the neutral. Our spectrum at 355 nm (Figure 2a) revealed partially resolved vibrational structures. The fact that no single vibrational progression was observed suggested that there is more than one active vibrational mode. Most likely, the bending and symmetric stretching modes were both active. This observation is consistent with the calculated structural changes between the anion and neutral ground state of FeS_2 by Schröder et al.[13] Interestingly, their calculated relative energies between the anion and neutral is 3.30 eV, which is in excellent agreement with our measured EA of 3.222 eV for FeS_2 (Table 2). However, the sharp spectral features observed in the *X* band did not suggest a large bond angle change as predicted by Schröder et al.

The EA of FeS_2 is quite high, suggesting that the FeS_2^- anion is very stable. This is understandable, because in FeS_2^- the Fe and S are both in their favorite oxidation state; i.e., FeS_2^- can be viewed as $S^{2-}Fe^{3+}S^{2-}$ in a formal sense. The five d electrons in Fe^{3+} are high spin coupled, giving rise to the $^6A_1$ ground state. The quintet ground state of FeS_2 ($^5B_2$) implies that the removed electron is mainly of Fe 3d character. The change of the Fe−S bond length suggests that there is significant covalent interaction between the Fe 3d orbitals and the S 3p. We note that the PES spectra of FeS_2^- are similar to those of its valent isoelectronic FeO_2^- species,[30,31] which also has a similar bent structure. However, it is surprising that the EA of FeS_2 is even higher than that of FeO_2 (2.36 eV),[30,31] consistent with the fact that the Fe−S interaction is more covalent that the Fe−O bond.

The very weak feature (X′) observed at the lower binding energy side of the FeS_2^- spectrum (Figure 2a) is assigned to the triangular isomer of FeS_2^- with a S−S bond. The lower EA of this isomer is expected and is consistent with the theoretical calculation by Schröder et al.,[13] who predicted a vertical EA of 1.71 eV for the triangular isomer.

4.3. FeS_3^- to FeS_6^-: Electron Binding Energy Trend and Implication for Structural Evolution. The 355 nm PES spectrum of FeS_3^- (Figure 3a) exhibited a simple vibrational progression with a frequency of 500 cm^{-1}. This frequency is comparable to that of the diatomic FeS and should be due to an Fe−S symmetric stretching mode. The simple vibrational progression suggests that the ground states of FeS_3^- and FeS_3 may possess rather high symmetry. There are two possible structures, either a D_{3h} structure without any S−S bonding or a C_{2v} structure with one S−S bond, a $SFe(S_2)$ type of structure. In the D_{3h} structure, the 500 cm^{-1} mode would correspond to the totally symmetric stretching, whereas in the C_{2v} structure

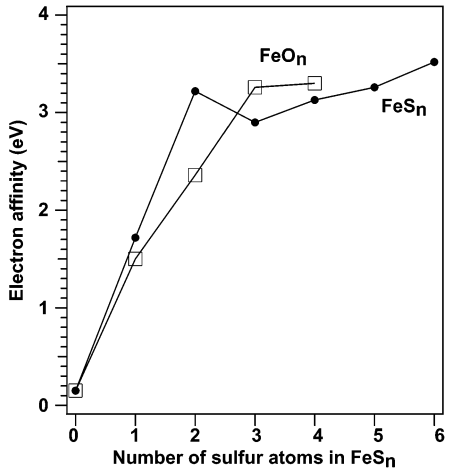

Figure 9. Electron affinities of FeS_n (filled dots) as a function of n compared to those of FeO_n from ref 31 (empty squares). The EA for Fe atom is taken from ref 40.

this mode could correspond to the stretching of the SFe moiety in $SFe(S_2)$. We expected that the D_{3h} structure would have a higher electron affinity, whereas the C_{2v} structure would have an EA comparable to that of FeS_2.

Interestingly, we observed that the EA of FeS_3 is even smaller than that of FeS_2 (Table 2). This is very different from the EA trend from FeO_2 to FeO_3, which exhibits a large increase from the EA of 2.36 eV for FeO_2 to 3.26 eV for FeO_3.[31] This was interpreted as a sequential oxidation, in that the Fe is further oxidized in FeO_3 relative to FeO_2, and a D_{3h} structure was proposed for FeO_3.[31] The current observation of a decrease in EA from FeS_2 to FeS_3 suggests that the Fe is not further oxidized in the latter, favoring the C_{2v} structure for FeS_3. This is understandable because oxygen is expected to be a stronger oxidizer and the Fe−O bond is expected to be more ionic than the Fe−S bond. Therefore, Fe prefers its favorite +3 oxidation state in FeS_3^-, which can be viewed formally as $S^{2-}Fe^{3+}(S_2^{2-})$.

Figure 7 shows all the PES data of FeS_n^- ($n = 1-6$) at 193 nm. We note that the electron binding energies of the larger clusters ($n > 3$) are in general similar to those of FeS_2^- and FeS_3^-. Figure 9 plots the trend of the EA as a function of n for FeS_n, compared with that of FeO_n.[31] It is clear that the EAs of FeS_{4-6} are similar to that of FeS_2 without any significant increase, suggesting that Fe is likely to maintain its favorite +3 oxidation state in all these clusters with $(S_m^{2-})Fe^{3+}(S_{n-m}^{2-})$ types of structures. For example, FeS_4^- may be either $S_2^{2-}Fe^{3+}S_2^{2-}$ or $S^{2-}Fe^{3+}S_3^{2-}$. The trend of the EA for the FeO_n series is consistent with the above structural evolution. The EA of FeO_4 is similar to that of FeO_3, suggesting the onset of an O−O unit in FeO_4^-, which was experimentally confirmed.[31] In the following section, we present a preliminary DFT calculations, which generally confirm the above structural evolution for the larger FeS_n^- clusters.

4.4. Preliminary DFT Calculations. Accurate prediction of various electronic states of Fe−S systems is a considerable challenge to computational chemistry, due to the existence of near degenerate states and low-lying geometrical isomers. We are interested in a detailed understanding of the electronic structure and chemical bonding of Fe−S clusters using DFT. Although detailed calculations will be presented in a forthcoming paper,[32] here we wish to report structural results from our DFT calculations. DFT has been very successful in electronic structure calculations of transition metals and had become a default choice.[33] Despite this phenomenal success, DFT is still a single determinant method and cannot account for static correlation effects, arising from near degenerate electronic states, which are important for Fe−S systems. Therefore, our aim in the current preliminary study is to identify various low-lying isomers of FeS_n^-, which can be used later for more accurate calculations.

All calculations were done with ADF[34,35] at the level of generalized gradient approach using Perdew−Wang exchange-correlation functional[36,37] at the unrestricted level. Slater-type-orbital (STO) basis sets of triple-ζ plus polarization (TZP) functions were used for both Fe and S atoms without any frozen core approximation (i.e., all electron calculations). The geometries of all the molecules were fully optimized with the default parameters.

Structures of the two low-lying isomers for each FeS_n^- species are presented in Figure 10, along with their relative energies and bond lengths. We first examine the DFT results for FeS^-. In contrast to the $^4\Delta$ ground state of FeO^-,[30,38,39] calculations by Hubner et al. gave a $^6\Delta$ ground state for FeS^- with a 2.16 Å bond length.[25] Our DFT calculations also predict the $^6\Delta$ ground state for FeS^- with a bond length of 2.13 Å and a configuration of $10\sigma^2 4\pi^4 11\sigma^1 5\pi^2 1\delta^3 12\sigma^1$. However, both our calculations and the previous DFT calculations with large basis set predict a $^5\Delta$ ground state for FeS.[25] According to our study,

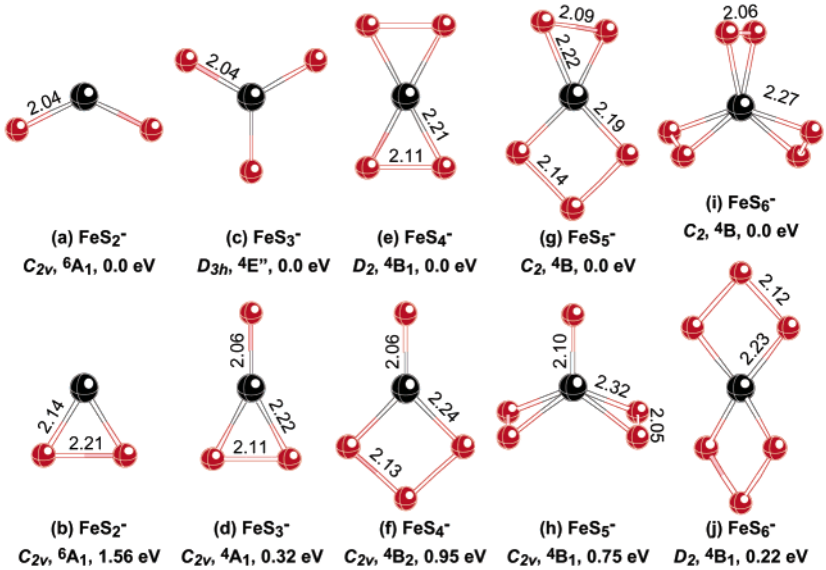

Figure 10. Structures and low-lying isomers of FeS_n^- ($n = 2-6$) from density functional calculations.

the highest singly occupied molecular orbitals of FeS^- are the $1\delta\ \beta$ and $12\sigma^1\ \alpha$ MOs, which are closely spaced. Detachment from the 12σ and 1δ MOs results in the $^5\Delta$ ground state and the $^7\Sigma^+$ excited state of FeS, respectively, consistent with our spectral assignments.

However, ground state predictions become more complicated for other members of the series. Not only various electronic states but also different geometrical isomers become competitive. For FeS_2^-, we obtained a bent ground state (Figure 10a), which is in agreement with the previous DFT calculations by Schröder et al.[13] The triangular isomer (Figure 10b) is about 1.56 eV higher in energy. For FeS_3^-, our DFT calculations gave two isomers (Figure 10c,d) very close in energy, with the D_{3h} structure (Figure 10c) slightly more stable than the C_{2v} isomer (Figure 10d). It is not clear which one is the ground state, because it is well-known that DFT overestimates the stabilization of delocalized structures, but the C_{2v} isomer is consistent with our experimental results. For both FeS_4^- and FeS_5^-, our calculations give the D_2 (Figure 10e) and C_2 (Figure 10g) ground states, which are more stable than the closest isomers by 0.95 and 0.75 eV, respectively. However, the two isomers for FeS_6^- (Figure 10i,j) are very close in energy, making it difficult to ascertain which one is the ground state.

One important feature that distinguishes between oxides and sulfides is that the sulfides are more covalent. Our preliminary charge analyses of the FeS_n^- series indicate that there is little charge polarization among the Fe and S atoms. Overall, the DFT results are consistent with the $(S_m^{2-})Fe^{3+}(S_{n-m}^{2-})$ types of structures proposed on the basis of the experimental results. A detailed theoretical study on the FeS_n^- clusters is forthcoming.[32]

5. Conclusions

In conclusion, we report a photoelectron spectroscopic investigation of a series of monoiron−sulfur clusters FeS_n^- ($n = 1-6$) at four photon energies. Vibrationally resolved spectra were obtained for FeS^- and FeS_3^-, and well-resolved spectra with numerous features were obtained for all FeS_n^- species. Detailed electronic energy level information is obtained for FeS from the PES data of FeS^- and tentative assignments are presented. Sequential oxidation of Fe was observed only for the first two S atoms, where each S atom is responsible for a large increase of electron affinity of ∼1.6 and ∼1.5 eV, respectively. All larger species FeS_n ($n = 3-6$) were observed to possess electron affinities similar to that of FeS_2 within ±0.3 eV. On the basis of the EA trend, a general structural evolution scheme is proposed, where all FeS_n^- ($n > 1$) species take the $(S_m^{2-})Fe^{3+}(S_{n-m}^{2-})$ type structures, in which Fe maintains its favorite +3 oxidation state. Preliminary DFT calculations were carried out, which, in general, verify the proposed structural types for FeS_n^-.

Acknowledgment. We thank Dr. Jun Li for invaluable discussions and assistance in the theoretical calculations. This research was supported by the National Institutes of Health (GM-63555) and partially by the Petroleum Research Fund, administered by the American Chemical Society. The experiment was performed at the W. R. Wiley Environmental Molecular Sciences Laboratory, a national scientific user facility sponsored by DOE's Office of Biological and Environmental Research and located at Pacific Northwest National Laboratory, operated for DOE by Battelle. All the calculations were performed using supercomputers at EMSL MSCF.

References and Notes

(1) Beinert, H.; Holm, R. H.; Munck, E. *Science* **1997**, *277*, 653.
(2) Ogino, H.; Inomata, S.; Tobita, H. *Chem. Rev.* **1998**, *98*, 2093.
(3) Harris, S. *Polyhedron* **1989**, *8*, 2843.
(4) Noodleman, L.; Peng, C. Y.; Case, D. A.; Mouesca, J.-M. *Coord. Chem. Rev.* **1995**, *144*, 199.
(5) Mouesca, J.-M.; Lamotte, B. *Coord. Chem. Rev.* **1998**, *178−180*, 1573.
(6) Wang, L. S.; Cheng, H. S.; Fan, J. J. *J. Chem. Phys.* **1995**, *102*, 9480. Wang, L. S.; Wu, H. In *Advances in Metal and Semiconductor Clusters. IV. Cluster Materials*; Duncan, M. A., Ed.; JAI Press: Greenwich, 1998; pp 299−343.
(7) Wang, L. S.; Ding, C. F.; Wang, X. B.; Barlow, S. E. *Rev. Sci. Instrum.* **1999**, *70*, 1957.
(8) DeVore, T. C.; Franzen, H. F. *High Temp. Sci.* **1975**, *7*, 220.
(9) Barsch, S.; Kretzschmar, I.; Schroder, D.; Schwarz, H.; Armentrout, P. B. *J. Phys. Chem. A* **1999**, *103*, 5925.
(10) Barsch, S.; Schroder, D.; Schwarz, H.; Armentrout, P. B. *J. Phys. Chem. A* **2001**, *105*, 2005.
(11) Hettich, R. L.; Jackson, T. C.; Stanko, E. M.; Freiser, B. S. *J. Am. Chem. Soc.* **1986**, *108*, 5086.
(12) Husband, J.; Aguirre, F.; Thompson, C. J.; Metz, R. B. *Chem. Phys. Lett.* **2001**, *342*, 75.
(13) Schroder, D.; Kretzschmar, I.; Schwarz, H.; Rue, C.; Armentrout, P. B. *Inorg. Chem.* **1999**, *38*, 3474.
(14) Carlin, T. J.; Wise, M. B.; Freiser, B. S. *Inorg. Chem.* **1981**, *20*, 2743.
(15) Dance, I.; Fisher, K.; Willett, G. *Angew. Chem., Int. Ed. Engl.* **1995**, *34*, 201.
(16) Dance, I.; Fisher, K.; Willett, G. *Inorg. Chem.* **1996**, *35*, 4177.
(17) MacMahon, T. J.; Jackson, T. C.; Freiser, B. S. *J. Am. Chem. Soc.* **1989**, *111*, 421.
(18) Yu, Z.; Zhang, N.; Wu, X.; Gao, Z.; Zhu, Q.; Kong, F.*J. Chem. Phys.* **1993**, *99*, 1765.
(19) Nakat, J. E.; Fisher, K. J.; Dance, I. G.; Willett, G. D. *Inorg. Chem.* **1993**, *32*, 1931.
(20) Zhang, N.; Hayase, T.; Kawamata, H.; Nakao, K.; Nakajima, A.; Kaya, K. *J. Chem. Phys.* **1996**, *104*, 3413. Nakajima, A.; Hayase, T.; Hayakawa, F.; Kaya, K. *Chem. Phys. Lett.* **1997**, *280*, 381.
(21) Anderson, A. B.; Hong, S. Y.; Smialek, J. L. *J. Phys. Chem.* **1987**, *91*, 4250.
(22) Bauschlicher, Jr., C. W.; Maitre, P. *Theor. Chim. Acta.* **1995**, *90*, 189.
(23) Bridgeman, A. J.; Rothery, J. *J. Chem. Soc., Dalton Trans.* **2000**, *2*, 211.
(24) Glukhovtsev, M. N.; Bach, R. D.; Nagel, C. J. *J. Phys. Chem. A* **1997**, *101*, 316.
(25) Hubner, O.; Termath, V.; Berning, A.; Sauer, J. *Chem. Phys. Lett.* **1998**, *294*, 37.
(26) Hubner, O.; Sauer, J. *J. Chem. Phys.* **2002**, *116*, 617.
(27) Wang, L. S.; Niu, B.; Lee, Y. T.; Shirley, D. A.; Balasubramanian, K. *J. Chem. Phys.* **1990**, *92*, 899.
(28) Akola, J.; Manninen, M.; Hakkinen, H.; Landman, U.; Li, X.; Wang, L. S. *Phys. Rev. B* **1999**, *60*, 11297.
(29) Wang, L. S.; Li, X. Temperature Effects in Anion Photoelectron Spectroscopy of Metal Clusters. In *Clusters and Nanostructure Interfaces*; Jena, P.; Khanna, S. N.; Rao, B. K., Eds.; World Scientific: New Jersey, 2000; p 293.
(30) Fan, J.; Wang, L. S. *J. Chem. Phys.* **1995**, *102*, 8714.
(31) Wu, H.; Desai, S. R.; Wang, L. S. *J. Am. Chem. Soc.* **1996**, *118*, 5296, 7434.
(32) Kiran, B.; Li, J.; Zhai, H. J.; Wang, L. S. Manuscript to be published.
(33) Ziegler, T. *Chem. Rev.* **1991**, *91*, 651.
(34) ADF 2002, SCM, Theoretical Chemistry, Vrije Universiteit, Amsterdam, The Netherlands (http://www.scm.com). te Velde, G.; Bickelhaupt, F. M.; van Gisbergen, S. J. A.; Guerra, C. F.; Baerends, E. J.; Snijders, J. G.; Ziegler, T. *J. Comput. Chem.* **2001**, *22*, 931.
(35) Guerra, C. F.; Snijders, J. G.; te Velde, G.; Baerends, E. J. *Theor. Chem. Acc.* **1998**, *99*, 391.
(36) Perdew, J. P.; Wang, Y. *Phys. Rev. B* **1992**, *45*, 13244.
(37) Perdew, J. P.; Chevary, J. A.; Vosko, S. H.; Jackson, K. A.; Pederson, M. R.; Singh, D. J.; Foilhais, C. *Phys. Rev. B* **1992**, *46*, 6671.
(38) Dolg, M.; Wedig, U.; Stoll H.; Preuss, H. *J. Chem. Phys.* **1987**, *86*, 2123.
(39) Krauss, M.; Stevens, W. J. *J. Chem. Phys.* **1985**, *82*, 5584.
(40) Leopold, D. G.; Lineberger, W. C. *J. Chem. Phys.* **1986**, *85*, 51.